High Resolution 3-D Angle of Arrival Determination for Indoor UWB Multipath Propagation

Yongwei Zhang, *Member, IEEE,* Anthony K. Brown, *Senior Member, IEEE,* Wasim Q. Malik, *Member, IEEE,* and David J. Edwards

***Abstract*—Propagation measurements using a large array are used to study the angle of arrival (AOA) across the ultrawideband (UWB) frequency range of 3.1 to 10.6 GHz. A two-dimensional Unitary ESPRIT algorithm is employed to give a high resolution estimation of AOA including both the azimuth and elevation angles of multipath components. The frequency dependence of AOA is investigated over the UWB frequency band. The multipath rays form clusters in both angular and temporal domains. Within a cluster the azimuth and elevation AOAs are determined to follow Laplacian and Gaussian distributions respectively. In the indoor environment considered, a typical cluster extends over an angular sector of approximately 14 degrees in azimuth and 9 degrees in elevation, with up to 5 clusters observed. We note that these propagation characteristics will allow UWB systems to utilise smart antennas or MIMO structures to improve overall throughput.**

***Index Terms*—Angle of arrival estimation, multipath scattering, ultrawideband (UWB), unitary ESPRIT.**

I. Introduction

THERE are several system design approaches to wireless communications that offer performance gains including the use of antenna diversity techniques to combat or take advantage of multipath effects. These approaches are closely tied to the physical propagation mechanisms of the environment and can be described by the angular spectrum of multipath [1], [2].

Propagation studies have been reported for narrowband indoor environments [3], [4], [5], [6]. For the UWB channel the spatial-temporal properties have been examined in [7], [8], [9], [10], where it is shown that the multipath components in the azimuth plane arrive in clusters. It has been reported in [7] that the relative azimuth arrival angles of the multipath components within any one cluster approximate to a Laplacian probability density function. However, the bandwidth involved in [7] is only 1.5 GHz and cannot typically represent the whole UWB frequency band. Measurements in a residential environment [8] found that the spread of the arrival angle of the main components of the line-of-sight (LOS) path is limited to about 10 degrees in azimuth; for the non-line-of-sight (NLOS) link, the distribution is wider but no particular conclusion was given. All of the above Angle Of Arrival (AOA) investigations were performed in one dimension only, i.e., it is assumed that the signals impinge from the horizontal plane. The consideration of elevation angle is important in an indoor environment since differences in the elevation distribution of received power can lead to significant changes in capacity of Multiple-Input Multiple-Output (MIMO) systems[11]. In general, it has been noted that local geometry and the building architecture can have a significant effect on the received signals [12]. The work reported here indicates new information for different environments and provides supplementary insight for the spatial characteristics of the indoor UWB channel, including the distribution of multipath arrivals in both azimuth and elevation domains.

Each ray path in a multipath channel will, in general, have its own impulse response [13], [14]. In order to clearly understand the propagation mechanisms behind the spatial-temporal characteristics of the multipath, a 3-D ray tracing model [15] has been employed and compared to the measured data. From this the complex reflection, refraction and diffraction of each multipath component are extracted providing physical insight into the propagation mechanism.

This paper is organised as follows: In Section II, a generic array measurement technique is introduced. Section III describes the AOA analysis algorithm. The frequency dependent AOA over the UWB band is presented in Section IV while Section V derives channel models characterizing the distribution of AOAs in both azimuth and elevation domains. Section VI concludes the paper.

II. Experiment Design and Measurement Apparatus

In this section, we give a brief review of the array measurement experimental technique used in the paper, which closely follows [9], [16], [17], [18].

The experiments were conducted in two rooms. We refer to them as "office 1" and "office 2" in the following analysis. The sizes of the rooms are 6 m $\times$ 6 m and 5.7 m $\times$ 4.8 m respectively. A probe antenna was accurately moved over a closely spaced grid of points, with phase and amplitude

Manuscript received November 24, 2006; revised April 6, 2007 and September 13, 2007; accepted December 2, 2007. The associate editor coordinating the review of this paper and approving it for publication was M. Shafi. This work has been supported by EPSRC and The University of Manchester.

Y. Zhang and A. K. Brown are with the School of Electrical and Electronic Engineering, The University of Manchester, Manchester, M60 1QD, U.K. (e-mail: david.zhang@ieee.org; anthony.brown@manchester.ac.uk).

W. Q. Malik is with the Department of Brain and Cognitive Sciences, Massachusetts Institute of Technology, Cambridge, MA. He is also with the Massachusetts General Hospital, Harvard Medical School, Harvard University, Boston, MA (e-mail: wqm@mit.edu).

D. J. Edwards is with the Department of Engineering Science, University of Oxford, Oxford, UK (e-mail: david.edwards@eng.ox.ac.uk).

Digital Object Identifier 10.1109/TWC.2008.060979.

Fig. 1. The measurement apparatus and environment.

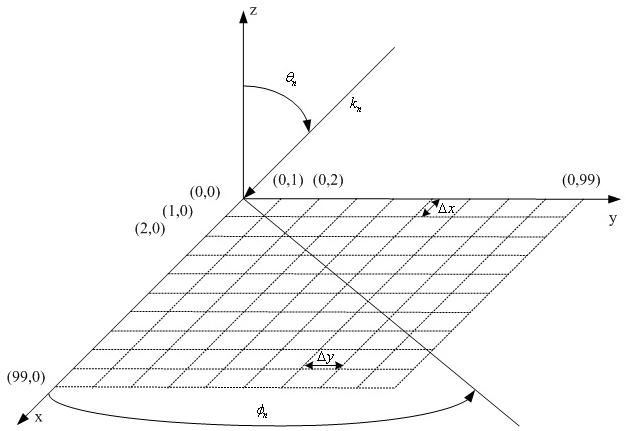

Fig. 2. Geometry of the rectangular array and definition of the angular parameters.

recorded over 1601 frequency points across the entire UWB band of 3.1 to 10.6 GHz at each spatial grid point. A square grid arrangement was used to form a virtual receiving array of size 100×100 elements with a uniform spacing of $d = 0.01$ m. The measurement apparatus as well as the layout of "office 2" is shown in Fig. 1. The system was calibrated prior to the measurement to remove frequency-dependent attenuation and phase distortion in the measurement apparatus. It is noted that the probe antenna effects are included in the measured data. Earlier work has shown that the effect of a probe antenna can be very significant in propagation channel measurement [19]. Therefore the antenna used here is based on the design reported in [20] having low antenna dispersion characteristics and only a dip in the vertical direction rather than a deep null. Line-of-sight (LOS) and Obstructed-line-of-sight (OLOS) measurements were conducted for "office 1" and only LOS measurement was performed for "office 2". The OLOS environment was created by placing a rectangular aluminium sheet (0.6 m $\times$ 1.2 m) between the transmit and receive antennas. The spherical coordinate system for the receiving array is shown in Fig. 2. At each grid location, the complex channel transfer function was recorded:

$$H(x, y, f) = a_{x,y,f} e^{j\gamma_{x,y,f}} \tag{1}$$

where $a_{x,y,f}$ and $\gamma_{x,y,f}$ are the measured magnitude and phase response at frequency f on grid position (x, y).

Post-processing allows the sequence of measurements composing the array to be interpreted as simultaneous measurements so that array processing can be used to analyze spatial properties of the channel. The underlying assumption is that the environment does not change while the sequence of measurements is being made and care was taken to ensure this. The fully filled "virtual array" measurement takes approximately 20 hours to complete. One advantage of this approach over using a physical array is that mutual coupling is avoided since only one antenna element is present.

III. Analysis Tool

The recovery of signal parameters from noisy observations is a fundamental problem in array signal processing. Due to their simplicity and high-resolution capability, ESPRIT-like (Estimation of Signal Parameters via Rotational Invariance Techniques) subspace estimation schemes [21], [22] have been attracting considerable attention. Applications of such technique allow AOA of individual multipath component to be extracted from measurement data. This information is significant for new access schemes, such as spatial division multiple access (SDMA), where enhanced concepts are employed to make use of AOA distributions [1], [2].

A. 2-D Unitary ESPRIT With Spatial Smoothing

The ESPRIT-like subspace estimation schemes obtain the parameter estimates by exploiting the rotational invariance structure of the signal subspace, induced by the translational invariance structure of the associated sensor array. This can be achieved without massive computation [21]. There are several versions of ESPRIT reported including LS (least squares), TLS (total least squares) and unitary ESPRIT [22].

A recently proposed direction finding algorithm 2-D Unitary ESPRIT [23], [24], [25], with 2-D spatial smoothing [26], estimates azimuth and elevation angle of arrival jointly from the outputs of a planar antenna structure. The algorithm provides increased resolution compared to conventional Fourier-based processing [9], [22] for a good signal-to-noise environment. The performance of Unitary ESPRIT is not affected by the correlation of the multipath components due to the inherent forward-backward averaging effect [23].

The algorithmic principle of 2-D Unitary ESPRIT is given in [23], [25]. Our work differs from the normal applications since we only measure a single "snapshot" of the channel response. This is solved by an extension of 2-D spatial smoothing [26]. The basic principle for this approach is discussed in [27], [28]. We measured an array of points as shown in Fig. 2 over the entire frequency band. This is a super spatial resolution data set (1 cm or approximately 0.33λ at the highest measurement frequency). We first extract a subarray with dimensions $(\tilde{N}_1, \tilde{N}_2)$ from the measurement data set. This is organized into a column vector $\mathbf{x}_1(\tau)$. Second subarray is then extracted which differs from the first by a shift of one column and one row with respect to the first subarray. These values are

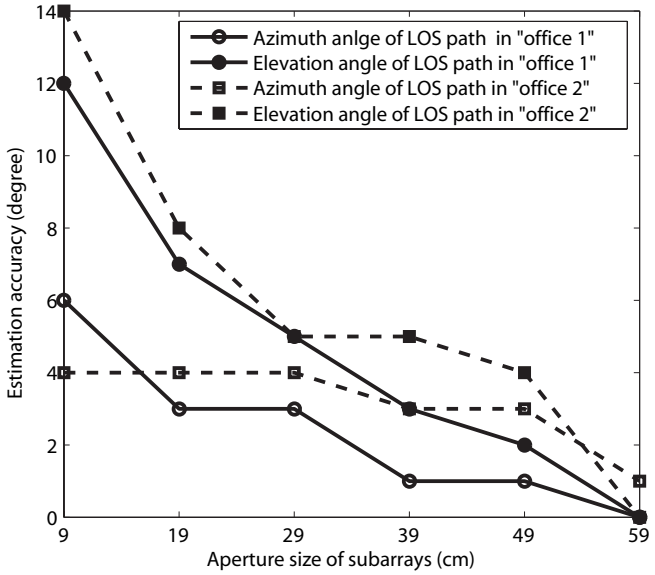

Fig. 3. The estimation accuracy of the ESPRIT algorithm with respect to the size of the subarray. The actual direction of the LOS path is known from the geometry of the environment model.

stacked into the column vector $\mathbf{x}_2(\tau)$. This process is repeated until we reach the end of whole array of measurement data. Finally, all the forward smoothing generated snapshots are grouped together to form the direct data matrix

$$\mathbf{X} = [\mathbf{x}_1(\tau), \mathbf{x}_2(\tau), \cdots, \mathbf{x}_{M_l}(\tau)] \tag{2}$$

where M_l represents the number of "snapshots." It has been shown that spatial smoothing not only allows the full rank of the covariance matrix to be restored, but also achieves superior performance when the arriving signals are correlated [26].

The size of the subarray has to be chosen with some care, normally the larger the subarray, the higher the available angular resolution. However this is only true if all sources are in the far field of the array. In general in indoor propagation, as shown in [9], sources may be either in the near field or far field. LOS sources are the closest to the array; other multipath may be considered as arriving from the images of the transmit antenna due to the reflections by the walls. To optimize accuracy and following [9], we established the largest subarray which did not show significant phase curvature from various multipath sources indicating these are essentially in the far field. This subarray was 60 points equivalent to subarray length of 59 cm. This array length gives the LOS source to be approximately $0.5D^2/\lambda$ at the centre band. Fig. 3 shows the estimation accuracy of the algorithm changes with the size of the chosen subarrays for the LOS paths at 3.1 GHz. Root Mean Square error (RMSE) is defined in (3) to measure the estimation accuracy. We note that the direction of the LOS path is known from the geometry of the setting. The ESPRIT algorithm accurately estimated this with the aperture length of 59 cm.

B. Error Estimation of 2-D Unitary ESPRIT

To evaluate the errors from the ESPRIT algorithm, a data set was constructed assuming four multipath arrivals, each multipath of equal power. Simulations were conducted employing a 100×100 Uniform Rectangular Array (URA) with $\Delta_x = \Delta_y = 0.01$ m. The frequency for the evaluation is 6.5 GHz. The incoming directions used are $(\phi, \theta) = (45^o, 80^o)$, $(\phi, \theta) = (100^o, 45^o)$, $(\phi, \theta) = (200^o, 5^o)$, and $(\phi, \theta) = (300^o, 90^o)$. The Root Mean Square error (RMSE) of i^{th} source is then

$$RMSE_i = \sqrt{(\hat{\phi}_i - \phi_i)^2 + (\hat{\theta}_i - \theta_i)^2}, \quad i = 1, 2, 3, 4 \tag{3}$$

where $\hat{\phi}_i$, $\hat{\theta}_i$ are the estimated azimuth and elevation angles from the ESPRIT algorithm, ϕ_i and θ_i are the "perfect" angular locations of the corresponding multipath. The array data sets were constructed based on different signal-to-noise ratio (SNR) values [29]. In this simulation, the noise is assumed white Gaussian with the noise power controlled at different levels with respect to the signal power received across the array. In addition to this four-source scenario, various runs of multipath combination (including different number and angular arrival directions) were carried out. The simulation results show that the error estimations in the elevation angles from the ESPRIT algorithm are the dominant contributions to the RMSE. The estimation error is within 6 degrees when the SNR is over 10 dB and it is less than 4 degrees when the SNR is greater than 15 dB. As we would expect from projected aperture effects, the RMSE of the signals coming from the lower elevation angle ($\theta = 80^o$ and $\theta = 90^o$) is higher than the signals coming from the higher elevation angle ($\theta = 45^o$ and $\theta = 5^o$).

It should be noted here that the accuracy of the AOA estimation may vary with frequency. Note that the electrical size of the measurement array and the separation of the measured points changes with frequency as they are physically fixed at 1 m $\times$ 1 m and 1 cm respectively. This effect will be discussed in Section IV. Furthermore, interactions with scatterers and the antenna radiation pattern can also cause distortions and show frequency-selective characteristics [9], [13], [20], [30]. This may lead to lower SNR for the frequency sensitive multipath components resulting in inaccuracy in AOA estimation by the algorithm.

IV. Measured Angle of Arrival for UWB Channel in Different Frequency Bands

The 2-D unitary ESPRIT algorithm steps described in the above section were applied on measured channel response data across the UWB frequency band. At each measurement position 1601 frequency points were measured from 3.1 GHz to 10.6 GHz (that is separated by 4.7 MHz). The spectrum of multipath arrivals across the frequency band derived from the ESPRIT algorithm is represented by a matrix $\mathbf{A}$ of rank (n, L), where n is the number of frequency points, L is the maximum number of multipath components. The elements of matrix $\mathbf{A}$ are the estimated power for the arrived multipath components. The angular properties were stored in two associated matrixes, $\mathbf{\Phi}$ and $\mathbf{\Theta}$, where $\mathbf{\Phi}$ is the azimuth angle and $\mathbf{\Theta}$ the elevation.

For the "office 1" case, the estimated results of the multipath angular spectrum is given in Fig. 4 in LOS case. In practice, the entire UWB frequency band is split into two subbands

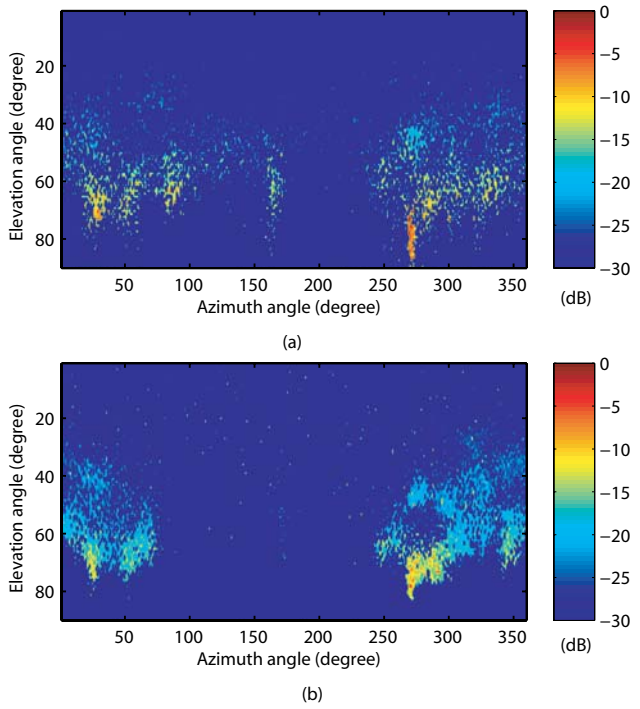

Fig. 4. The average angular spectrum of multipath propagation across the UWB band for the LOS case in the "office 1" scenario. (a) The low frequency band 3.1-4.85 GHz; (b) The high frequency band 6.2-9.7 GHz.

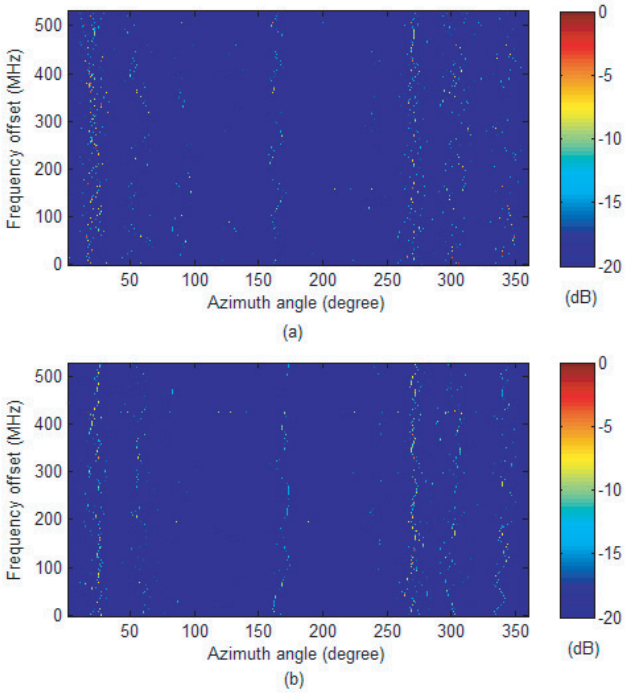

Fig. 5. AOA in the azimuth domain vs. the frequency offset in LOS case in the "office 1". (a) The frequency offset is from 3.1 GHz in the low frequency band; (b) The frequency offset is from 6.2 GHz in the high frequency band.

due to technological possibilities [31], [32], the low frequency band from 3.1 GHz to 4.85 GHz and the high frequency band from 6.2 GHz to 9.7 GHz. The angular spectrum for the multipath components is averaged over each subband. It is observed that the multipath rays form clusters in the angular domain. There are various definitions of "clusters" in the literature (e.g. [33]). We define a cluster here as a group of multipath components with similar AOA and absolute time delay. As was noted in [7], there are difficulties in developing a robust algorithm for the automatic identification of multipath clusters. We therefore identify clusters manually by considering the number of occurrence of angular arrival across the frequency band. Based on this, considering the low band, multipath components were clustered with the AOA of the centre of the clusters in the azimuth domain at $\phi = \mathbf{25}^o$, $\phi = \mathbf{95}^o$, and $\phi = \mathbf{270}^o$. For the high band, a significant difference in the angular spectrum was observed with the cluster centres being $\phi = \mathbf{25}^o$, $\phi = \mathbf{270}^o$ and $\phi = \mathbf{345}^o$. Considering just the main multipath components, i.e., those within 10 dB of the peak received power (see Fig. 4), the cluster centres of $\phi = \mathbf{25}^o$ and $\phi = \mathbf{270}^o$ appear at both bands. Within the low frequency band, the components with azimuth AOA close to $\mathbf{168}^o$ are not considered sufficiently differentiated to be included in the analysis.

The frequency bandwidth of the two subbands considered above is large, i.e., 1.75 GHz for the low band and 3.5 GHz for the high band. To provide greater insight a detailed analysis was undertaken over a 528 MHz window within each subband. Following the metric suggested in [34], the angular spectrum of multipath components is plotted against frequency offset using a 4.7 MHz increment from the lowest frequency point in each case. This is shown in Fig. 5. It is derived from the measured data using the modified ESPRIT algorithm for the LOS case in the "office 1". The azimuth AOAs of the arriving multipath components are plotted over the frequency window for the same receiving array with the transmitting source at a fixed location. It is observed that the variation in the AOA of the dominant multipath components is insignificant over the frequency window of 528 MHz. The AOA variations over frequency for within either subband or between subbands are of the same order.

The properties of AOA of the multipath are usefully presented as their Probability Density Function (PDF). In the azimuth angle domain, the following expression is used

$$p(\phi) = \sum_{i=1}^{Q} \sum_{m=1}^{L} S(f_i, \phi_{i,m})/Q \tag{4}$$

where $S(f_i, \phi_{i,m}) = \mathbf{1}$ when the azimuth AOA for multipath number "m", $\phi_{i,m}$, is equal to the reference azimuth angle ϕ at the observed frequency, f_i, otherwise $S(f_i, \phi_{i,m}) = \mathbf{0}$, L is the total number of multipath components, Q is the number of frequency samples in the operation band. Similarly, the elevation AOA can be characterized by

$$p(\theta) = \sum_{i=1}^{Q} \sum_{m=1}^{L} S(f_i, \theta_{i,m})/Q \tag{5}$$

The PDF of AOA in the azimuth domain for the low and high frequency band in the "office 1" scenario is given in Fig. 6. There are clearly two main "clusters" where the mean azimuth AOA are $\mathbf{25}^o$ and $\mathbf{270}^o$.

For the "office 2" case, the PDF of azimuth AOA is shown in Fig. 7. There are five clusters identified in the low frequency band. Equal number of clusters has been found in the high

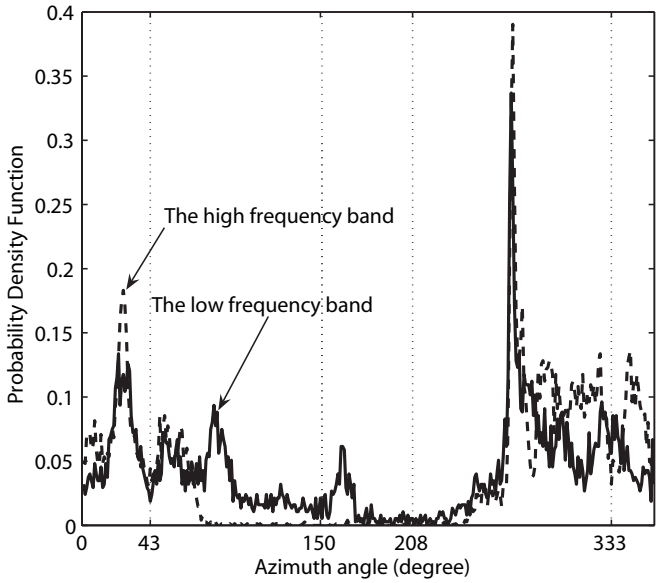

Fig. 6. The probability density function of relative azimuth angle of arrival for LOS condition at the "office 1." The low frequency band is from 3.1 to 4.85 GHz; the high frequency band is from 6.2 to 9.7 GHz.

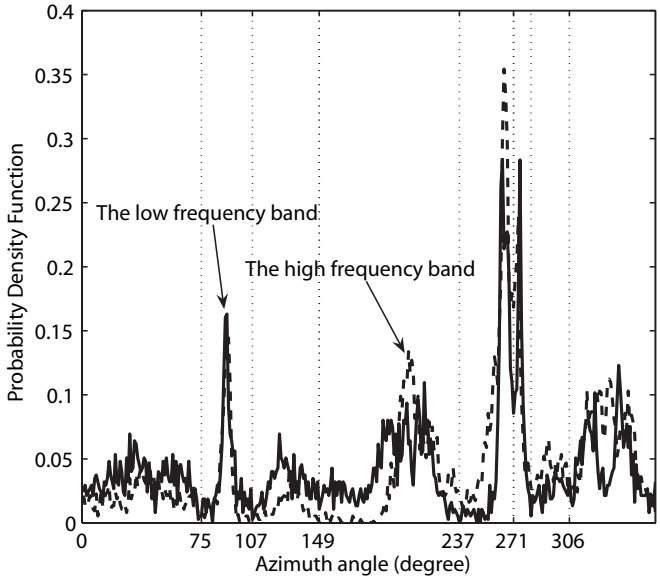

Fig. 7. The probability density function of relative azimuth angle of arrival for LOS condition at the "office 2." The low frequency band is from 3.1 to 4.85 GHz; the high frequency band is from 6.2 to 9.7 GHz.

frequency band, but only three from the same directions as the low frequency band results. We note the clusters from $\phi = 265^o$ and $\phi = 275^o$ are very close in space, but they have different TOA. Ray tracing analysis (see Section V-C) shows one of these is a direct LOS path; the other one is a reflected path from the wall right behind the transmitter.

V. Numerical Results

A. The Distribution of Azimuth Angle of Arrival

The channel model used to describe the angular impulse response is given in [5] as:

$$h(\phi) = \sum_{l=0}^{\infty} \sum_{k=0}^{\infty} \beta_{kl} \delta(\phi - \Phi_l - \omega_{kl}) \qquad (6)$$

where β_{kl} is the amplitude of the k^{th} arrival in the l^{th} cluster, Φ_l is the mean azimuth AOA of the l^{th} cluster and ω_{kl} is the azimuth AOA of the k^{th} arrival in the l^{th} cluster relative to Φ_l. Based on the above analysis of AOA for the two UWB frequency bands, β_{kl} is a strong frequency dependent value in some directions. The above model is therefore inaccurate as it assumes each ray path is independent of frequency. Therefore by modifying the above expression, a more accurate expression for the angular impulse response has the following form

$$h(\phi, f) = \sum_{l=0}^{\infty} \sum_{k=0}^{\infty} \beta_{kl}(f) \delta(\phi - \Phi_l - \omega_{kl}) \qquad (7)$$

The recovered rays across the UWB frequency band by 2-D Unitary ESPRIT were tested against Laplacian density functions. For "office 1" case, the azimuth distribution of relative AOA of resolved rays with respect to the cluster mean were shown in Fig. 8 for the LOS case and in Fig. 9 for the OLOS case. For the LOS case in "office 1", low and high band data are a good fit to a Laplacian density function, with standard deviation $\delta = 14^o$ and $\delta = 9^o$ respectively; for OLOS in the same office, standard deviation $\delta = 27^o$ and $\delta = 11^o$ also show a good fit. For the "office 2" scenario, the parameters of the best fit Laplacian are $\delta = 11^o$ for the low frequency band and $\delta = 14^o$ for the high frequency band.

Reference [6] and [7] reports standard deviations of a Laplacian density function of $\delta = 25.5^o$, $\delta = 21.5^o$ for two different buildings and $\delta = 38^o$ for an office/laboratory environment. The difference suggests that the parameter is likely a function of building architecture. However, the conclusion from [6] was achieved by rotating a parabolic dish antenna with a null to null beamwidth of 10^o, whereas an array antenna was used in [7], the size of array being used is 7×7 with 6 inches spacing. The angular resolution of these measurement systems would be limited by the beamwidth in [6] and accuracy of the CLEAN algorithm in [7].

In summary, the differences of the parameters between previously reported scenarios are affected by the bandwidth of UWB signals and the time resolution the measurement equipment allow. There may also be a difference in the methodology to identify clusters although this is unclear in previously published literature. Based on the high resolution measurements undertaken in this paper, the parameters for the Laplacian distribution of the azimuth AOA derived from 2-D ESPRIT for the two office rooms are given in Table I.

B. The Distribution of Elevation Angle of Arrival

Using the same principles derived for azimuth angle estimation technique we evaluate the properties of AOA in the elevation domain. Here we see the PDF of elevation AOA is not a good fit to a Laplacian function, it is however well represented by a Gaussian function. This characteristic can also be observed from the ray tracing results. These results are in contrast to the distribution of the angular spread at the base station in mobile communication systems in the outdoor environment [35] where a Laplacian function is used to model angular dispersion in both the horizontal and vertical planes.

In the current results, the different AOA distribution in the azimuth and elevation domains relates to the physical structure

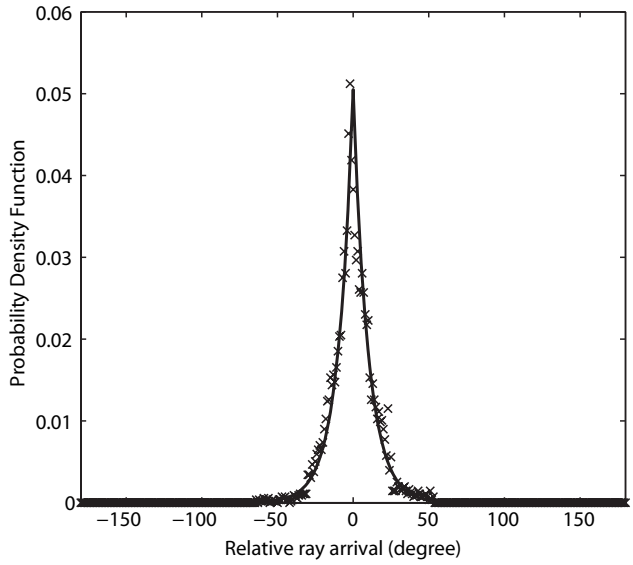

(a)

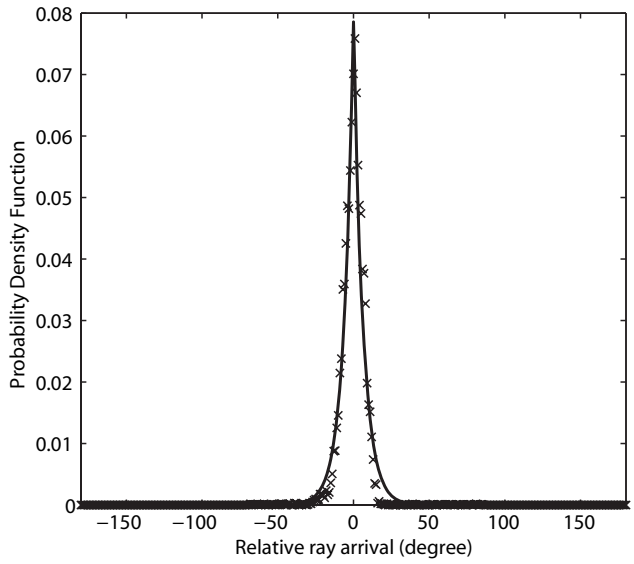

(b)

Fig. 8. The ray azimuth angle of arrival and best fit Laplacian density distribution in "office 1" based on LOS. (a) The low frequency band 3.1-4.85 GHz with parameter $\boldsymbol{\delta = 14^o}$; (b) The high frequency band 6.2-9.7 GHz with parameter $\boldsymbol{\delta = 9^o}$.

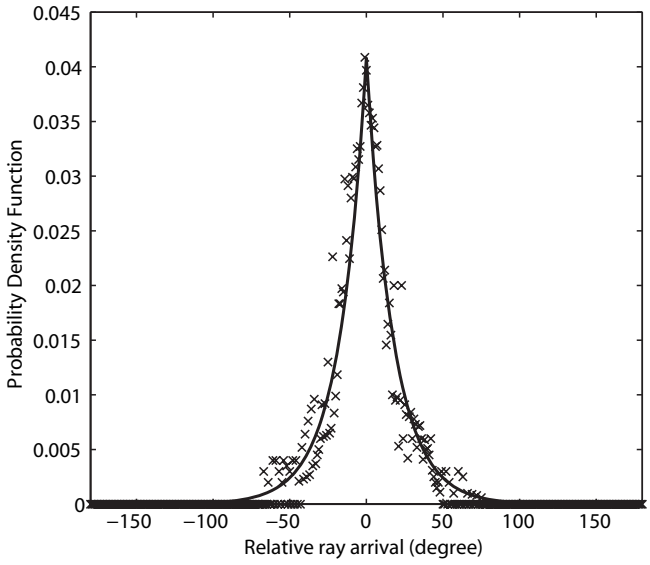

(a)

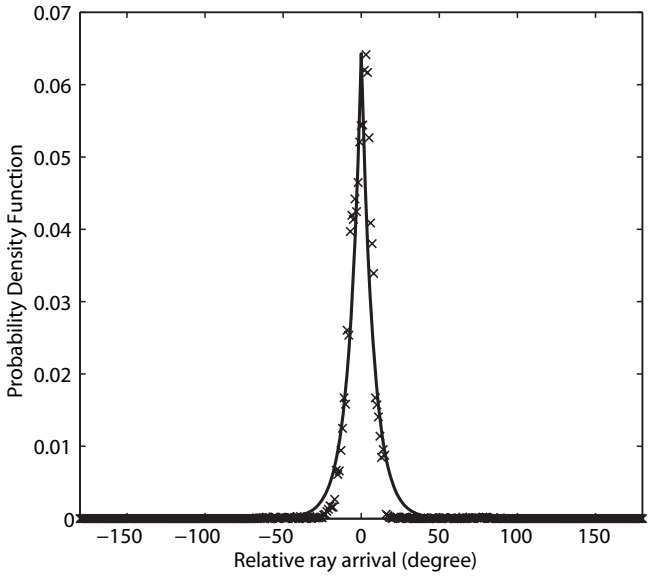

(b)

Fig. 9. The ray azimuth angle of arrival and best fit Laplacian density distribution in "office 1" based on OLOS. (a) The low frequency band 3.1-4.85 GHz with parameter $\boldsymbol{\delta = 27^o}$; (b) The high frequency band 6.2-9.7 GHz with parameter $\boldsymbol{\delta = 11^o}$.

of the measured indoor environment, which is different in the two planes. Another possible effect is the probe antenna radiation pattern, however this is not considered to be significant unless rays are arriving from very high angles (close to zenith) due to the radiation pattern of the probe antenna. Such high angle rays are not evident in the ray tracing simulation or the measurement estimations. The distribution of elevation AOA for "office 1" case and its best fit Gaussian function is shown in Fig. 10. The parameters of the Gaussian distribution are $\boldsymbol{\delta = 10^o}$ and $\boldsymbol{\delta = 8^o}$ for the low and high frequency band respectively. In the "office 2", the parameter of Gaussian distribution for both the low and high frequency band is $\boldsymbol{\delta = 9^o}$. The parameters for the elevation AOA distribution together with the azimuth AOA are summarized in Table I.

C. Scattering Mechanisms of the Multipath Propagation

In this section, we employ 3-D ray tracing techniques [15] to identify the individual scattering mechanism involved in the propagation of the individual ray path. The ray tracing used here inherently provides time delay, angle of arrival, and the scattering information for multipath reception conditions. A typical case of diffraction scattering is given in Fig. 11. The impulse response of the multipath propagation and their corresponding AOAs are described in Fig. 12.

For the measured data, the time domain response of the channel is derived from the frequency domain measurement. The impulse response function of the multipath channel within the first 15 ns excess time delay for the "office 1" scenario is shown in Fig. 12 for the receiving point at the centre of measurement array. The predicted result from the ray tracing

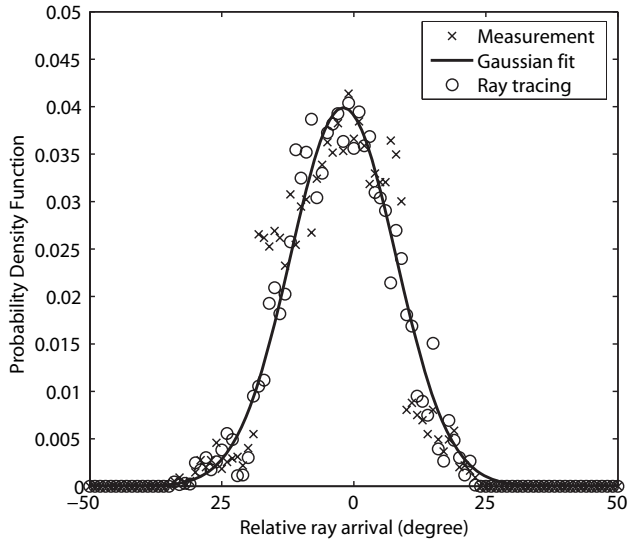

(a)

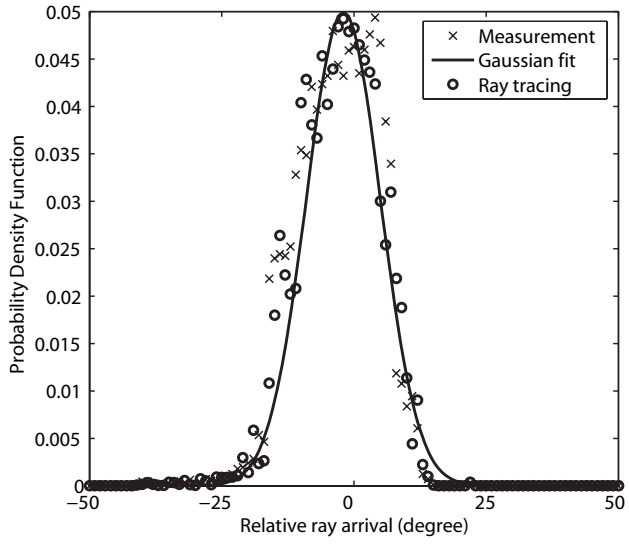

(b)

Fig. 10. The ray elevation angle of arrival and the best fit Gaussian density function in the "office 1" based on LOS. (a) The low frequency band 3.1-4.85 GHz with parameter $\boldsymbol{\delta = 10^o}$; (b) The high frequency band 6.2-9.7 GHz with parameter $\boldsymbol{\delta = 8^o}$.

TABLE I
PARAMETERS FOR THE AOA DISTRIBUTION MODELS

Parameters for Azimuth Angle Laplacian Distribution					
		Low band		High band	
		LOS	OLOS	LOS	OLOS
Office 1	$\boldsymbol{\delta(deg)}$	14	27	9	11
Office 2	$\boldsymbol{\delta(deg)}$	LOS		LOS	
		11		14	

Parameters for Azimuth Angle Laplacian Distribution					
		Low band		High band	
		LOS	OLOS	LOS	OLOS
Office 1	$\boldsymbol{\delta(deg)}$	10	9	8	7
Office 2	$\boldsymbol{\delta(deg)}$	LOS		LOS	
		9		9	

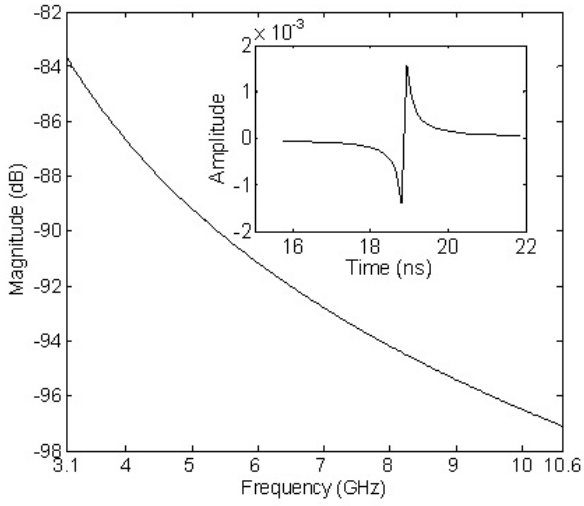

Fig. 11. The frequency-dependent diffraction scattering around a 90 degrees curved wedge in "office 1." The results are based on UTD with finitely conducting straight wedges. The small window is the corresponding time domain response by IFFT.

model is also given in the figure, which are in generally good agreement. Ray tracing as noted on the figure identifies the azimuth AOA and the scattering mechanisms corresponding to the individual multipath component. It is seen that the LOS ray from $\phi = \mathbf{270^o}$ and single-reflection rays from $\phi = \mathbf{25^o}$ contribute the main multipath components. The two-time-reflection rays from $\phi = \mathbf{262^o}$ and $\phi = \mathbf{276^o}$ are partially overlapped with excess time delay between 7 ns and 8 ns. Another two multipath components with $\phi = \mathbf{166^o}$ and $\phi = \mathbf{160^o}$ arrive the receiver at the excess time delay $\boldsymbol{t = 11.63}$ ns and $\boldsymbol{t = 13.37}$ ns respectively, and both having two-time reflections during propagation.

There are three diffracted rays identified in the first 15 ns time window by the ray tracing model, with excess time delay of $\boldsymbol{t = 3.91}$ ns, $\boldsymbol{t = 8.71}$ ns and $\boldsymbol{t = 12.02}$ ns and corresponding AOAs are $\phi = \mathbf{338^o}$, $\phi = \mathbf{330^o}$ and $\phi = \mathbf{45^o}$. One of these ($\phi = \mathbf{338^o}$) is of significant amplitude and can be clearly seen in the measured data. The other two diffracted rays are not explicitly seen in the measurement due to their high attenuation. The simulated diffraction scattering for the $\phi = \mathbf{338^o}$ ray is given in Fig. 11. In this, the diffraction is at a straight wedge consisting of finitely conducting material with relative dielectric constant $\boldsymbol{\epsilon_r = 7.9}$ and loss tangent $\boldsymbol{\delta = 0.7}$. Fig. 11 also demonstrates the time domain response of the diffracted component. The strong frequency-dependent character was shown on this ray path.

A comprehensive comparison between the ray-tracing results and the measurement results indicates that the complex scattering mechanisms, which occur within indoor multipath propagation, can be predicted to reasonable accuracy. We also note that rays from different AOA can arrive very close in time and those with close AOA can have different TOA. This is important when considering antenna diversity techniques such as MIMO.

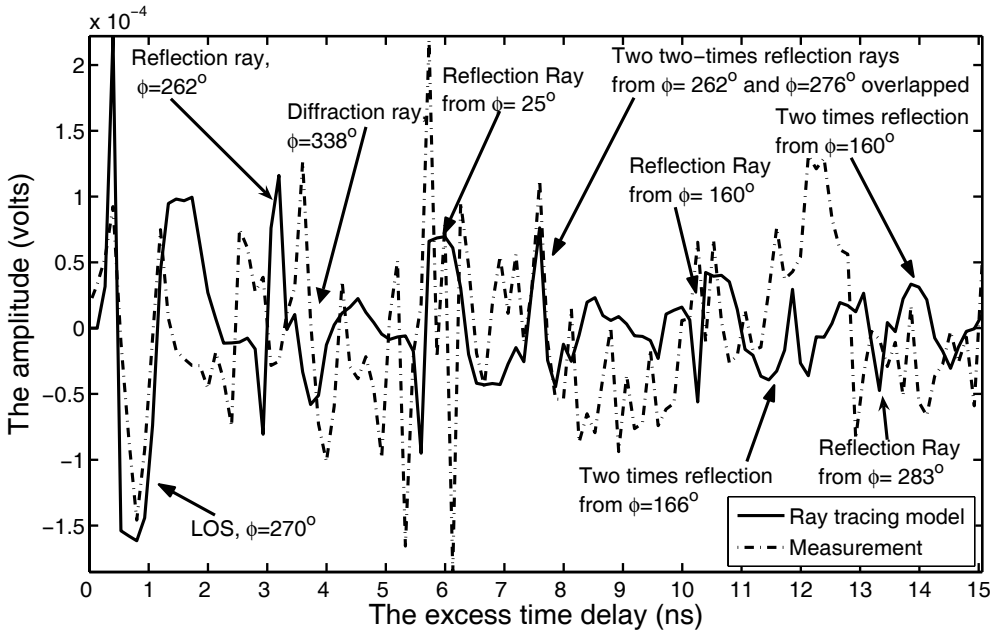

Fig. 12. The scattering mechanisms of the individual multipath propagation and Azimuth AOA.

VI. Conclusions

Multipath clustering in both azimuth and elevation for an indoor UWB propagation channel has been investigated. The results presented show a Laplacian PDF is a good match for the distribution of relative azimuth AOA. This agrees with the previous reported results in principle, however the Laplacian parameters are somewhat different. This, we believe, is due to both different environment and the improved accuracy of the new technique. The relative elevation AOA distribution function is first reported in this paper and this follows a Gaussian, not Laplacian distribution within a cluster. We split the entire UWB spectrum into two subbands in keeping with practical systems. The high frequency band, which has a broader frequency bandwidth, does not correspond to a significant larger standard deviation of relative angle-of-arrival. This indicates that the large scale building features determine the angular arrivals of higher power multipath components. It should be noted that the parameters of the AOA distribution are dependent on room geometries. Larger array apertures, dense element spacing and using a high resolution algorithm have resulted in more ray arrival clusters being identified than might have been expected from previous literature.

References

[1] A. F. Molisch, *Wireless Communications*. John Wiley & Sons, Ltd., 2005.

[2] B. Allen, M. Dohler, E. Okon, W. Malik, A. Brown, and D. Edward, *Ultra Wideband Antennas and Propagation for Communications, Radar, and Imaging*. Wiley, 2006.

[3] A. A. M. Saleh and R. A. Valenzuela, "A statistical model for indoor multipath propagation," *IEEE J. Select. Areas Commun.*, vol. 5, no. 2, pp. 128–137, Feb. 1987.

[4] H. Hashemi, "Impulse response modeling of indoor radio propagation channels," *IEEE J. Select. Areas Commun.*, vol. 11, no. 7, pp. 967–978, Sept. 1993.

[5] Q. Spencer, M. Rice, B. Jeffs, and M. Jensen, "A statistical model for the angle-of-arrival in indoor multipath propagation," in *Proc. IEEE Veh. Technol. Conf.*, May 1997, vol. 3, pp. 1415–1419.

[6] Q. Spencer, B. Jeffs, M. Jensen, and A. Swindlehurst, "Modelling the statistical time and angle of arrival characteristics of an indoor multipath channel," *IEEE J. Select. Areas Commun.*, vol. 18, no. 2, pp. 347–360, Mar. 2000.

[7] R. J.-M. Cramer, R. A. Scholtz, and M. Z. Win, "Evaluation of an ultra-wide-band propagation channel," *IEEE Trans. Antennas Propagat.*, vol. 50, no. 5, pp. 561–570, May 2002.

[8] L. Rusch, C. Prettie, D. Cheung, Q. Li, and M. Ho, "Characterization of uwb propagation from 2 to 8 ghz in a residential environment," [online]. Available: http://www.intel.com/technology/comms/uwb/

[9] W. Q. Malik, C. J. Stevens, and D. J. Edwards, "Synthetic aperture analysis of multipath propagation in the ultra-wideband communications channel," in *Proc. IEEE Signal Proc. Advances Wireless Commun.*, June 2005, pp. 375–379.

[10] K. Haneda, J. Takada, and T. Kobayashi, "Clusterization analysis of spatial-temporal UWB radio channel for line-of-sight and non-line-of-sight indoor home environments," in *Proc. Joint COST 273/284 Workshop Antennas and Related System Aspects Wireless Commun.*, June 2004.

[11] M. Shafi, M. Zhang, P. J. Smith, A. L. Moustakas, and A. F. Molisch, "The impact of elevation angle on mimo capacity," in *Proc. IEEE ICC*, June 2006, pp. 4155–4160.

[12] T. S. Rappaport, S. Y. Seidel, and K. Takamizawa, "Evaluation of an ultra-wide-band propagation channel," *IEEE Trans. Commun.*, vol. 39, no. 5, pp. 794–807, May 1991.

[13] R. C. Qiu, "A study of the ultra-wideband wireless propagation channel and optimum UWB receiver design," *IEEE J. Select. Areas Commun.*, vol. 20, no. 9, pp. 1628–1637, Dec. 2002.

[14] R. C. Qiu and I.-T. Lu, "Multipath resolving with frequency dependence for wide-band wireless channel modelling," *IEEE Trans. Veh. Technol.*, vol. 48, no. 1, pp. 272–285, Jan. 1999.

[15] Y. Zhang and A. K. Brown, "Ultra-wide bandwidth communication channel analysis using 3-d ray tracing," in *Proc. 1st International Symposium Wireless Commun. Syst.*, Sept. 2004, pp. 443–447.

[16] W. Q. Malik, D. J. Edwards, and C. J. Stevens, "Experimental evaluation of rake receiver performance in a line-of-sight ultra-wideband channel," in *Proc. Joint IEEE Ultra-Wideband Sys. Tech. & Int. Workshop Ultra-Wideband Syst.*, May 2004, pp. 217–220.

[17] J. Liu, B. Allen, W. Q. Malik, and D. J. Edwards, "On the spatial correlation of MB-OFDM ultra wideband transmissions," in *Proc. COST 273 Meeting*, Jan. 2005.

[18] M. Steinbauer, A. F. Molisch, and E. Bonek, "The double-directional radio channel," *IEEE Antennas Propagat. Mag.*, vol. 43, no. 4, pp. 51–63, Aug. 2001.

[19] Y. Zhang and A. K. Brown, "The discone antenna in a BPSK direct-

sequence indoor UWB communication system," *IEEE Trans. Microwave Theory Techniques*, vol. 54, no. 4, pp. 1675–1680, Apr. 2006.
[20] W. Q. Malik, C. J. Stevens, and D. J. Edwards, "Angular-spectral antenna effects in ultra wideband communication links," *IEE Proc.-Commun.*, vol. 153, no. 1, pp. 99–106, Feb. 2006.
[21] R. Roy and T. Kailath, "Esprit-estimation of signal parameters via rotational invariance techniques," *IEEE Trans. Acoust., Speech Signal Processing*, vol. 37, no. 7, pp. 984–995, July 1989.
[22] H. L. V. Trees, *Optimum Array Processing, Part IV of Detection, Estimation, and Modulation Theory*. John Wiley & Sons, Inc., New York, 2002.
[23] M. Haardt and J. A. Nossek, "Unitary esprit: How to obtain increased estimation accuracy with a reduced computational burden," *IEEE Trans. Signal Processing*, vol. 43, no. 5, pp. 1232–1242, May 1995.
[24] M. D. Zoltowski, M. Haardt, and C. Mathews, "Closed-form 2-d angle estimation with rectangular arrays in element space or beamspace via unitary esprit," *IEEE Trans. Signal Processing*, vol. 44, no. 2, pp. 316–328, Feb. 1996.
[25] M. Haardt, M. D. Zoltowski, C. Mathews, and J. A. Nossek, "2-d unitary esprit for efficient 2-d parameter estimation," in *Proc. International Conf. Acoust., Speech, Signal Processing*, May 1995, vol. 3, pp. 2096–2099.
[26] S. U. Pillai and B. H. Kwon, "Forward/backward spatial smoothing techniques for coherent signal identification," *IEEE Trans. Acoust., Speech Signal Processing*, vol. 37, no. 1, pp. 8–15, Jan. 1989.
[27] J. E. Evans, J. R. Johnson, and D. F. Sun, "High resolution angular spectrum estimation techniques for terrain scattering analysis and angle of arrival estimation," in *Proc. 1st ASSP Workshop Spectral Esitmat.*, Aug. 1981, pp. 134–139.
[28] ——, "Application of advanced signal processing techniques to angle of arrival estimation in atc navigation and surveillance system," M.I.T Lincoln Lab., Lexington, MA, Rep. 582, 1982.
[29] N. Kikuma, *Adaptive Antenna Technology*. Ohmsa, Ltd., Oct. 2003.
[30] Y. Zhang and A. K. Brown, "Complex multipath effects in uwb communication channels," *IEE Proc. Commun.*, vol. 153, no. 1, pp. 120–126, Feb. 2006.
[31] R. F. et al., "DS-UWB physical layer submission to 802.15 task group 3a," IEEE P802.15-04/0137r3, July 2004.
[32] A. F. Molisch, "Ultrawideband propagation channels-theory, measurement, and modeling," *IEEE Trans. Veh. Technol.*, vol. 54, no. 5, pp. 1528–1545, Sept. 2005.
[33] C. C. Chong, C. Tan, D. Laurenson, S. McLaughlin, M. Beach, and A. Nix, "A new statistical wideband spatio-temporal channel model for 5-ghz band wlan systems," *IEEE J. Select. Areas Commun.*, vol. 21, no. 2, pp. 139–150, Feb. 2003.
[34] M. Beach, B. Allen, and P. Karlsson, "Spatial channel characterization of for smart antenna solutions in fdd wireless networks," *IEEE Trans. Antennas Propagat.*, vol. 52, no. 1, pp. 252–262, Jan. 2004.
[35] A. F. Molisch and F. Tufvesson, *Digital Signal Processing for Wireless Communications Handbook in M. Ibnkahla (ed.)*. CRC Press, 2004.

Yongwei Zhang (S'05-M'07) received the B.Sc. degree in communication engineering from Jilin University, Changchun, P. R. China, in 1996, and Ph.D. degree in electrical engineeging from the University of Manchester in 2007. In 1996, he joined Lucent Technologies, where he worked as a system engineer on 5ESS and PHS (Personal Handy-Phone System) systems. In 1998, he worked at Bell Labs, Naperville, U.S.A, on communication system engineering tools development. In his career at Lucent Technologies from 1996 to 2003, he had been involved in personal-handy-phone system network design and optimization. He had experience on adaptive array antenna design (TDMA/FDMA) and optimization for PHS systems. He joined the University of Manchester from 2003 in the Microwave and Communication Systems research group. His current research interests are mainly concerned with UWB communication system engineering including channel modelling, system performance analysis, UWB antenna design, and Square Kilometer Array (SKA) antenna design.

Tony Brown (M'91-SM'07) joined the University of Manchester in May 2003 as head of the Microwave and Communication Systems research group. Professor Brown has over 30 years of research and development into microwave antennas, communications, and radar systems. Starting work at GEC-Marconi Research Laboratories (1974) he worked on early satellite communications satellites including the 19 metre beam waveguide Goonhilly IV ground station. After a period with STL (Harlow) working on a variety of topics including adaptive and microstrip antennas, he was the first Racal Research Fellow on Telecommunications at the University of Surrey in 1980. He joined Racal full time in 1983, mainly working on military communications. He has been involved in cellular radio from the initial deployment in the UK and extensively in mobile satellite communications.

In 1987 Professor Brown founded Easat, a successful civilian radar supplier, where he remains as Chairman. Professor Brown was a founding member of the EPSRC Communications College. He is a Senior Member of the IEEE, and a Fellow of the IEE and of the Institute of Mathematics and its Applications (IMA). He is a UK representative to the European Union COST ASSIST initiative, a recent past member of the FCC Technical Advisory Commission (TAC), and is a past Chairman of the UK Chapter of the Applied Computational Electromagnetics Society (ACES). Professor Brown lectures in communications systems and in radar. His current research interests include ultra wide band antennas and propagation, large scale CEM, radio astronomy instrumentation, cross system interference issues, secure high frequency networks, and intelligent antennas.

Wasim Q. Malik (S'97, M'05) received the BE degree from the National University of Sciences and Technology, Pakistan, in 2000, and the DPhil degree from the University of Oxford, UK, in 2005, both in electrical engineering.

From 2005 to 2007, he was a Research Fellow at the University of Oxford, UK, and a Junior Research Fellow in Science at Wolfson College, Oxford. Since 2007, he has been a Postdoctoral Fellow at the Massachusetts Institute of Technology, USA.

Dr. Malik received the ESU Lindemann Science Fellowship 2007, the Best Paper Award at the ARMMS RF & Microwave Conference 2006, and the Association for Computing Machinery Recognition of Service Award 2000. He is an editor of the book *Ultra-Wideband Antennas and Propagation for Communications, Radar and Imaging* (UK: Wiley, 2006), and a Guest Editor of the *IET Microwaves Antennas and Propagation* special issue on "Antenna systems and propagation for future wireless communications" (Dec. 2007). He routinely serves on the organizing and technical program committees of various international conferences. He has published in excess of 60 papers in refereed journals and conferences.

David Edwards is a Professor of Engineering Science and Fellow of Wadham College Oxford. He holds a BSc, MSc and PhD in Physics, the Physics of Materials and Engineering from the University of Bristol, UK. After 12 years spent in industry (British Telecom), he returned to academia and has been an academic for 22 years (four years at Bristol University, 18 years at Oxford University). He has been in receipt of a number of awards and prizes in recognition of his work and has a strong record of innovation in communications systems, techniques, and technologies. He has published in excess of 300 publications during his time as an academic and has been extremely well supported by funding from research councils, industry, and government agencies. His current research areas include communications, antennas and propagation, electromagnetics, ad hoc networks, MIMO systems, and materials for electromagnetic applications. Professor Edwards has been awarded a number of patents and several have appeared as licensed commercial products. He has acted as a consultant to a large number of industrial organisations during his career, and has served on a number of national and international committees relating to the antennas and propagation fields, and continues to act as an industrial consultant in these areas. Prof. Edwards is a Chartered Engineer, a Fellow of the IET, and a Fellow of the Royal Astronomical Society.